DOI: 10.1002/ejic.200700297

New Reactivity of 4-Amino-3,5-bis(pyridin-2-yl)-1,2,4-triazole: Synthesis and Structure of a Mononuclear Species, a Dinuclear Species, and a Novel Tetranuclear Nickel(II) Rectangle Box, and Magnetic Properties of the Dinuclear and Tetranuclear Complexes

Ming-Liang Tong,*[a] Chao-Gang Hong,[a] Ling-Ling Zheng,[a] Meng-Xia Peng,[a,b] A. Gaita-Ariño,[c] and Juan Modesto Clemente Juan*[c]

Keywords: Nickel / Polynuclear / Azides / Magnetic properties

Reactions of $Ni(O_2CMe)_2·4H_2O$ or $NiCl_2·6H_2O$, 4-amino-3,5-bis(pyridin-2-yl)-1,2,4-triazole (abpt) and NaN_3 or KSCN in different molar ratios heated under reflux or hydrothermal conditions generate a mononuclear species with dimorphous phases, a dinuclear species incorporating an in situ deaminated [bpt-H]$^-$ ligand and a tetranuclear rectangle box incorporating an unprecedented $\mu:\eta^1:\eta^2:\eta^1$ coordination mode of the deprotonated [abpt-H]$^-$ ligand. Structural analysis reveals that a pair of $[Ni_2(\mu_{1,1}\text{-}N_3)(\mu\text{-}OAc)]$ motifs in $[Ni_4(abpt)_2(abpt\text{-}H)(N_3)_5(O_2CMe)_2]·5H_2O$ (**1**) are bridged by two abpt and one [abpt-H]$^-$ units into a rectangle box. $[Ni_2(bpt\text{-}H)_2(SCN)_2(H_2O)_2]·2H_2O$ (**2**) is a neutral centrosymmetric dinuclear Ni^{II} complex doubly bridged by abpt ligands. The complex $[Ni(abpt)_2(N_3)_2]$ (**3**) is a neutral centrosymmetric mononuclear Ni^{II} complex and crystallizes in polymorphous phases, showing an interesting example of temperature-induced polymorphism. Variable-temperature magnetic susceptibility measurements reveal that the ferromagnetic interaction via the $(\mu_{1,1}\text{-}N_3)_2(\mu\text{-}OAc)$ and $(\mu_{1,1}\text{-}N_3)(\mu_{1,1}\text{-}NH_{abpt-H})(\mu\text{-}OAc)$ bridges slightly dominates over the antiferromagnetic interaction via the abpt bridges, therefore indicative of an overall ferromagnetic coupling between Ni^{II} centers in **1**, and a moderate antiferromagnetic interaction occurs in **2**.

Introduction

Magnetic multimetal-centered complexes or metal clusters have attracted much attention over the past decades.[1,2] 4-Amino-3,5-bis(pyridin-2-yl)-1,2,4-triazole (abpt) is a potential multitopic ligand and its coordination chemistry has been investigating since the mid 1980s.[3] In particular, the spin-crossover system $[Fe(abpt)_2(X)_2]$ (where X = SCN^-, $SeCN^-$ or $N(CN)_2^-$, $TCNQ^-$) has been structurally and magnetically characterized.[4] So far, many coordination compounds of adpt have been synthesized.[5a,5b] However, most of them are mononuclear, particularly, only two examples of dinuclear nickel and copper complexes have been structurally characterized before our work,[3,5c] which indicate that the majority of these coordination compounds have relatively poor crystallization behavior in common solvents. This urged us to pursue its chemical reactivity under relatively unconventional conditions. We have recently been investigating a few in situ metal–organic reactions targeting a magnetic cluster system and furnished an interesting sandwich-type high-spin heterometallic $Ni_{12}K_4$ cluster from the reaction of di-2-pyridyl ketone with nickel acetate and azide in the presence of potassium *tert*-butoxide as a catalytic base.[6] Herein we report a tetranuclear rectangle box, a dinuclear complex and a mononuclear complex in polymorphous phases, which are synthesized by reflux and hydrothermal methods, respectively. They are $[Ni_4(abpt)_2(abpt\text{-}H)(N_3)_5(O_2CMe)_2]·5H_2O$ (**1**), $[Ni_2(bpt\text{-}H)_2(SCN)_2(H_2O)_2]·2H_2O$ (**2**) (bpt-H = 3,5-di-2-pyridyl-1,2,4-triazolate), α-$[Ni(abpt)_2(N_3)_2]$ (**3α**), and β-$[Ni(abpt)_2(N_3)_2]$ (**3β**). The [abpt-H]$^-$ in **1** resulted from the deprotonation of abpt during the reflux conditions and [bpt-H]$^-$ in **2** was formed from the deamination of abpt under solvothermal conditions.

[a] MOE Key Laboratory of Bioinorganic and Synthetic Chemistry, State Key Laboratory of Optoelectronic Materials and Technologies, School of Chemistry and Chemical Engineering, Sun Yat-Sen University,
Guangzhou, 510275 P. R. China
Fax: +86-20-8411-2245
E-mail: tongml@mail.sysu.edu.cn
[b] Department of Chemistry, Jiaying University,
514015 Meizhou, P. R. China
[c] Instituto de Ciencia Molecular, Universidad de Valencia,
C/ Dr. Moliner 50, 46100 Burjassot, Spain
E-mail: juan.m.clemente@uv.es

Results and Discussion

Synthesis and Characterization

In the reported metal complexes of the abpt ligand,[5a] the azide anion has not been chosen as the counterions, the azide salt is, therefore, introduced into the reaction system.

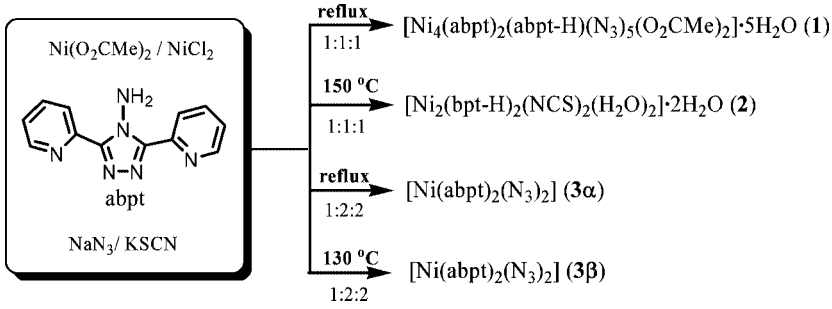

Scheme 1. Synthesis of **1**, **2**, **3α**, and **3β**.

The reaction of $Ni(O_2CMe)_2·4H_2O$, NaN_3 and abpt in a 1:1:1 molar ratio heated at reflux generated tetranuclear complex **1** (Scheme 1). When NaN_3 was replaced by KNCS, the solvothermal reaction of $NiCl_2·6H_2O$, KNCS and abpt in a 1:1:1 molar ratio led to dinuclear complex **2**. Remarkable is the deamination of abpt into bpt during the reaction probably related to the extreme conditions of the solvothermal reaction, which was also observed in the hydrothermal reaction of $[Co(abpt)_2(SCN)_2]$[3d] with $CoCl_2$. Furthermore, reactions of $NiCl_2·6H_2O$, NaN_3 and abpt in a 1:2:2 molar ratio heated at reflux or under solvothermal conditions led to the polymorphous mononuclear complexes of **3α** and **3β**, respectively, demonstrating that the factor of reaction temperature notably affects the final products. It should be noted that **3α** and **3β** are the first examples of ternary metal–abpt–azide complexes.

In addition to the bands of the abpt and $[abpt\text{-}H]^-$ ligands, the points of interest in the IR spectrum of the four complexes lie mainly in the bands due to the N_3^- or SCN^- groups. For **1**, the asymmetrical stretch $\nu_{as}(N_3)$ appears as strong bands at ca. 2070 and 2041 cm^{-1}, which is in good agreement with the existence of terminal and EO bridging azides in **1**; bands of weak intensity at about 1301 and 1284 cm^{-1} can be ascribed to the azide symmetric stretch $\nu_s(N_3)$. Very strong bands corresponding to the characteristic ν_{as} of the azido ligands appeared at 2034 cm^{-1} for **3α** and at 2053 cm^{-1} for **3β**. For **2**, the stretching vibration of the SCN^- group appears as a doublet at 2108 and 2058 cm^{-1}.

Crystal Structure

Single-crystal X-ray structure analysis revealed that **1** is a neutral tetranuclear Ni^{II} complex. A perspective view of the core part of **1** with the atom-labeling scheme is shown in Figure 1. Selected metric parameters associated with the nickel(II) center in **1** are given in Table 1. Each asymmetric unit of **1** contains four Ni^{II} atoms, two abpt ligands, one anionic $[abpt\text{-}H]^-$ ligand, five N_3^- ligands, two acetate ligands, and five lattice water molecules. Each Ni^{II} atom is in a distorted octahedral $[NiN_5O]$ environment, of which the coordination sphere for Ni1 or Ni2 is formed by two pyridyl N atoms, one triazole N atom, one azide N atom, one amine N atom, and one acetate O atom [Ni–N = 2.001(3)–2.166(3), Ni–O = 2.050(3) and 2.052(2) Å, *cis* N–Ni–N/O = 77.53(12)–103.06(12)°, *trans* N–Ni–N/O = 166.59(12)–176.55(13)°], while the coordination sphere for Ni3 or Ni4 is formed by one pyridyl N atom, one triazole N atom, three azide N atoms, and one acetate O atom [Ni–N = 2.062(4)–2.179(3), Ni–O = 2.047(3) and 2.053(3) Å, *cis* N–Ni–N/O = 76.55(12)–105.20(12)°, *trans* N–Ni–N/O = 167.27(12)–173.10(13)°]. The Ni1 and Ni2 are triply bridged by one μ-amino [Ni–N_{amino}–Ni = 97.74(14)°], one $\mu_{1,1}$-azide [Ni–N_{azide}–Ni = 88.92(12)°], and one μ-carboxylate-O,O′ with the Ni···Ni distance of 3.0253(8) Å and the Ni3 and Ni4 are triply bridged by two $\mu_{1,1}$-azides [Ni–N_{azide}–Ni = 95.74(13) and 98.39(15)°] and one μ-carboxylate-O,O′ with the Ni···Ni distance of 3.138(1) Å. The Ni1 and Ni4/Ni2 and Ni3 are each singly triazole-bridged with the Ni···Ni

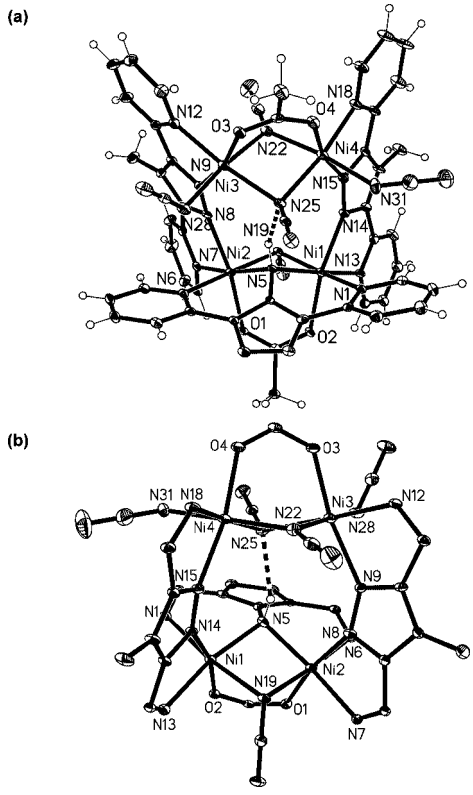

Figure 1. ORTEP plots of the molecular structure (a) and the connectivity pattern (b) in **1**. The methyl group and some of the carbon atoms of the pyridyl groups are omitted for clarity. 50% thermal ellipsoids are shown.

Table 1. Selected interatomic contacts [Å] and bond angles [°] for **1**.

Ni1–N5	2.015(3)	Ni3–O3	2.053(3)	Ni2–N19	2.154(3)	Ni4–N15	2.117(3)
Ni1–O2	2.052(2)	Ni3–N12	2.072(3)	Ni1···Ni2	3.0253(8)	Ni3···Ni4	3.1377(8)
Ni1–N13	2.095(3)	Ni3–N22	2.074(3)	Ni1···Ni4	4.578(1)	Ni2···Ni3	4.6680(9)
Ni1–N14	2.116(3)	Ni3–N28	2.079(4)	N5···N25	2.871(4)	O2w···N30	2.919(5)
Ni1–N1	2.122(3)	Ni3–N25	2.123(3)	N11···N27[b]	3.055(6)	O3w···O2w[d]	2.889(6)
Ni1–N19	2.166(3)	Ni3–N9	2.179(3)	N11···O4w	2.898(6)	O3w···N33[g]	2.892(7)
Ni2–N5	2.001(3)	Ni4–O4	2.047(3)	N17···O4w[c]	2.895(7)	O4w···O6w[a]	2.98(1)
Ni2–O1	2.050(3)	Ni4–N31	2.062(4)	N17···N30[d]	3.099(6)	O4w···O3w	2.733(6)
Ni2–N7	2.089(3)	Ni4–N22	2.071(4)	O1w···N3[e]	2.989(4)	O5w···N33	2.896(6)
Ni2–N6	2.092(3)	Ni4–N18	2.086(3)	O1w···N2	2.948(5)	O6w···O4w	2.91(1)
Ni2–N8	2.100(3)	Ni4–N25	2.108(3)	O2w···N19[f]	3.075(5)		
N5–Ni1–O2	90.3(1)	O3–Ni3–N12	91.1(1)	O1–Ni2–N6	87.6(1)	N31–Ni4–N18	96.2(1)
N5–Ni1–N13	168.0(1)	O3–Ni3–N22	91.8(1)	N7–Ni2–N6	97.3(1)	N22–Ni4–N18	91.5(1)
O2–Ni1–N13	89.5(1)	N12–Ni3–N22	93.6(1)	N5–Ni2–N8	96.2(1)	O4–Ni4–N25	88.5(1)
N5–Ni1–N14	103.1(1)	O3–Ni3–N28	91.0(1)	O1–Ni2–N8	169.7(1)	N31–Ni4–N25	92.0(1)
O2–Ni1–N14	166.6(1)	N12–Ni3–N28	93.3(1)	N7–Ni2–N8	78.9(1)	N22–Ni4–N25	80.4(1)
N13–Ni1–N14	77.5(1)	N22–Ni3–N28	172.5(1)	N6–Ni2–N8	87.3(1)	N18–Ni4–N25	171.8(1)
N5–Ni1–N1	91.2(1)	O3–Ni3–N25	86.8(1)	N5–Ni2–N19	82.7(1)	O4–Ni4–N15	167.3(1)
O2–Ni1–N1	88.7(1)	N12–Ni3–N25	173.1(1)	O1–Ni2–N19	92.7(1)	N31–Ni4–N15	86.2(1)
N13–Ni1–N1	100.8(1)	N22–Ni3–N25	80.0(1)	N7–Ni2–N19	86.1(1)	N22–Ni4–N15	95.8(1)
N14–Ni1–N1	90.4(1)	N28–Ni3–N25	93.3(1)	N6–Ni2–N19	176.6(1)	N18–Ni4–N15	77.1(1)
N5–Ni1–N19	82.1(1)	O3–Ni3–N9	167.4(1)	N8–Ni2–N19	93.0(1)	N25–Ni4–N15	103.5(1)
O2–Ni1–N19	95.8(1)	N12–Ni3–N9	76.6(1)	N5–H5N···N25	148(3)	O2w–H2wb···N30	175(5)
N13–Ni1–N19	86.0(1)	N22–Ni3–N9	86.6(1)	N11–H11A···N27[b]	154(4)	O3w–H3wa···O2w[d]	156(6)
N14–Ni1–N19	86.8(1)	N28–Ni3–N9	92.2(1)	N11–H11B···O4w	176(5)	O3w–H3wb···N33[g]	160(5)
N1–Ni1–N19	171.9(1)	N25–Ni3–N9	105.2(1)	N17–H17A···O4w[c]	164(4)	O4w–H4wa···O6w[a]	174(5)
N5–Ni2–O1	93.1(1)	O4–Ni4–N31	89.2(1)	N17–H17B···N30[d]	153(4)	O4w–H4wb···O3w	148(5)
N5–Ni2–N7	167.5(1)	O4–Ni4–N22	90.4(1)	O1w–H1wa···N3[e]	166(4)	O5w–H5w···N33	167(5)
O1–Ni2–N7	92.9(1)	N31–Ni4–N22	172.4(1)	O1w–H1wb···N2	164(4)	O6w–H6wa···O4w	118(10)
N5–Ni2–N6	93.9(1)	O4–Ni4–N18	91.7(1)	O2w–H2wa···N19[f]	168(4)		

Symmetry codes: [a] $-x + 1, y, -z + 3/2$. [b] $x, -y + 1, z + 1/2$. [c] $x, -y + 2, z - 1/2$. [d] $x, y + 1, z$. [e] $-x, y, -z + 1/2$. [f] $x, y - 1, z$. [g] $x, -y + 2, z + 1/2$.

separations of 4.578(1) and 4.6680(9) Å, respectively. A rectangle box is formed through these bridges. It is noteworthy that the dihedral angles between the coordinated pyridyl groups and the triazolato ring for the abpt and [abpt-H]$^-$ motifs are quite different. They are 24.5 and 25.2° for the anionic noncoplanar [abpt-H]$^-$ ligand, 2.3 and 22.1° for one half coplanar abpt ligand, and 6.1 and 7.0 ° for another coplanar abpt ligand, implying that there are different magnetic exchanges via the coplanar abpt, half-coplanar abpt and noncoplanar [abpt-H]$^-$ bridges. A recently reported example related to **1** was found in a tetranuclear nickel(II) rectangle box in which the long edges are spanned by the pyrazolate and each short edge is spanned by an acetate and a $\mu_{1,1}$ azide. The resulting rectangle was further capped by a $\mu_{1,1,3,3}$ bridging ligand.[7]

It is noteworthy that **1** is the first structurally characterized polynuclear cluster of the anionic [abpt-H]$^-$ ligand, in which the deprotonated 4-amino group, rather than N1 of the triazole ring, is coordinated to the Ni^{II} ion, and the deprotonated amino group of the [abpt-H]$^-$ acts as a μ-bridge, and the resulting anionic [abpt-H]$^-$ ligand adopts an unprecedented $\mu:\eta^1:\eta^2:\eta^1$ coordination mode (Scheme 2d). Although the anionic [abpt-H]$^-$ form was previously found in [Rh^I(abpt-H)(diolefin)] (diolefin = 1,5-cyclooctadiene, 2,3-(tetrafluorobenzo)bicyclo[2.2.2]octatriene, or bicyclo-[2.2.1]heptadiene) based mainly on spectroscopic data[8a] and recently structurally characterized in [Rh(phen)$_2$(abpt-H)](PF$_6$)$_2$,[8b] it only plays a chelating role via the imine nitrogen and a pyridine nitrogen. The deprotonated amino group is also stabilized by a moderate N–H···N$_{azide}$ hydrogen bond [N···N = 2.871(4) Å, N–H···N$_{azide}$ = 148(3)°].

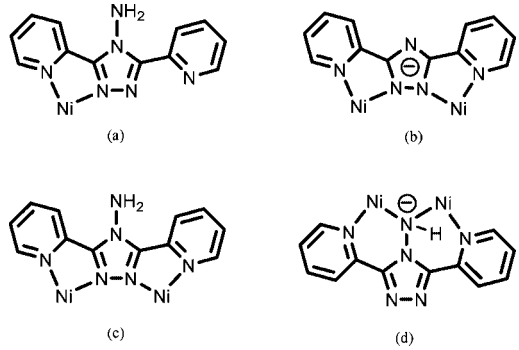

Scheme 2. Coordination modes of abpt (*a*, *c*), bpt-H (*b*), and abpt-H (*d*) in **1**, **2**, **3α**, and **3β**.

Compound **2** is a neutral centrosymmetric dinuclear Ni^{II} complex (Figure 2a). Each asymmetric unit of **2** contains one Ni^{II} atom, one anionic [bpt-H]$^-$ ligand, one SCN$^-$ ligand, one aqua ligand, and one lattice water molecule. The Ni^{II} atom is in a distorted octahedral [NiN$_5$O] environment. The four basal nitrogen atoms coordinated to the Ni^{II} atom belong to the pyridyl [N1 and N4a] and triazole [N2 and N3a] groups of two [bpt-H]$^-$ ligands. The Ni–N$_{pyridyl}$ distances are 2.220(2) and 2.193(2) Å (Table 2), respectively, which is slightly longer than those found in **1**; the

Ni–$N_{triazole}$ distances are 2.014(2) and 2.018(2) Å, respectively, which is shorter than those [2.110(3)–2.179(3) Å] found in **1**. The axial positions are occupied by one monodentate coordinating SCN^- anion [Ni–N6 = 2.044(3) Å] and one aqua ligand (Ni–O1w = 2.062(2) Å]. The dihedral angles between the coordinated pyridyl groups and the triazolato ring are 3.0 and 4.8°, respectively. It is noteworthy to mention that recently most of the discrete and polymeric metal complexes of $[bpt\text{-}H]^-$ have been structurally characterized,[9] which probably contributes to the fact that the hydro(solvo)thermal method was widely adopted in the preparations of new metal–organic frameworks in the past decade.[10] It is also interesting that the aqua ligands and the lattice water molecules form hydrogen-bonded cyclic water tetramers [O···O = 2.729(3) and 2.755(3) Å; O–H···O = 158(4) and 169(3)°], $(H_2O)_4$ with graph set notation of $R_4^2(8)$. Theoretical studies on the basis of ab initio electronic structure calculations predicted that the cyclic $(H_2O)_4$ clusters have several configurations, $R_4^4(8)$-types of D_{2h}, C_4, or S_4 symmetry and $R_4^3(8)$-type of C_s symmetry and most of them have widely been found in metal–organic frameworks and organic hosts.[11a,11b] The rare $R_4^2(8)$-type cyclic $(H_2O)_4$ tetramer was very recently found in an organic host.[11c] Each $(H_2O)_4$ tetramer in **2** is surrounded by four dinuclear species and each dinuclear species is surrounded accordingly by four $(H_2O)_4$ tetramers via the Ni–O coordination and O–H···N hydrogen-bonding interactions (Figure 2b).

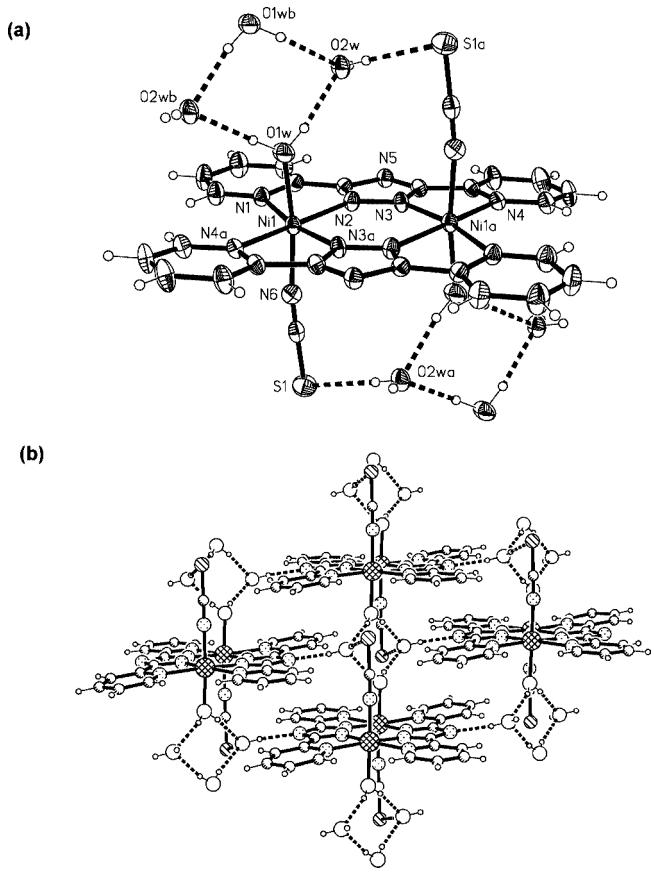

Figure 2. ORTEP plot of the molecule structure (a) and 2D hydrogen-bonded layer structure of **2**. 50% thermal ellipsoids are shown.

Table 2. Selected interatomic contacts [Å] and bond angles [°] for **2**.

Ni1–N2	2.014(2)	Ni1–O1w	2.062(2)
Ni1–N3[a]	2.018(2)	Ni1–N4[a]	2.193(2)
Ni1–N6	2.044(3)	Ni1–N1	2.220(2)
O1w···O2w[b]	2.755(3)	O2w···N5[c]	2.785(3)
O1w···O2w	2.729(3)	O2w···S1[a]	3.310(3)
N2–Ni1–N3[a]	92.12(9)	N6–Ni1–N4[a]	92.07(9)
N2–Ni1–N6	95.2(1)	O1w–Ni1–N4[a]	83.33(9)
N3[a]–Ni1–N6	94.94(9)	N2–Ni1–N1	75.94(9)
N2–Ni1–O1w	90.48(9)	N3[a]–Ni1–N1	167.99(8)
N3[a]–Ni1–O1w	90.1(1)	N6–Ni1–N1	87.60(9)
N6–Ni1–O1w	172.2(1)	O1w–Ni1–N1	88.7(1)
N2–Ni1–N4[a]	167.00(9)	N4[a]–Ni1–N1	115.18(8)
N3[a]–Ni1–N4[a]	76.52(8)	O2w–H2wb···N5[c]	173(4)
O1w–H1wa···O2w	158(4)	O2w–H2wa···S1[a]	178(4)
O1w–H1wb···O2w	169(3)		

Symmetry codes: [a] $-x, -y, -z$. [b] $-x, -y + 1, -z$. [c] $-x + 1, -y, -z$.

Both **3α** and **3β** are neutral centrosymmetric mononuclear Ni^{II} complexes. Their coordination geometries are quite similar. Each asymmetric unit of **3α** and **3β** contains one-half of a Ni^{II} atom, which lies on an inversion center, one abpt ligand, and one N_3^- ligand. The Ni^{II} atom is coordinated in a distorted octahedral $[NiN_6]$ environment. The four equatorial nitrogen atoms coordinated to the Ni^{II} atom belong to the pyridyl [N1 and N1a] and triazole [N2 and N2a] groups of two abpt ligands. The Ni–$N_{pyridyl}$ distance is 2.101(2) and 2.101(3) Å for **3α** and **3β**, respectively (Tables 3 and 4), which is slightly longer than those found in **1**; the Ni–$N_{triazole}$ distances are 2.039(2) and 2.053(3) Å for **3α** and **3β**, respectively, which is shorter than those [2.110(3)–2.179(3) Å] found in **1**. The remaining two *trans*

Table 3. Selected interatomic contacts [Å] and bond angles [°] for **3α**.

Ni1–N2	2.039(2)	Ni1–N7	2.126(2)
Ni1–N1	2.101(2)	N6···N9[b]	2.967(2)
N6···N4	2.848(2)		
N2–Ni1–N1[a]	101.32(6)	N1–Ni1–N7[a]	87.41(6)
N2–Ni1–N1	78.68(6)	N2–Ni1–N7	91.37(6)
N2–Ni1–N7[a]	88.63(6)	N1–Ni1–N7	92.59(6)
N6–H6a···N4	141(2)	N6–H6b···N9[b]	170(2)

Symmetry codes: [a] $-x, -y, -z$. [b] $x, y - 1, z$.

Table 4. Selected interatomic contacts [Å] and bond angles [°] for **3β**.

Ni1–N2	2.053(3)	Ni1–N7	2.126(3)
Ni1–N1	2.101(3)	N6···N9[b]	3.095(7)
N6···N4	2.863(5)		
N2–Ni1–N1	78.5(1)	N1–Ni1–N7[a]	89.8(1)
N2–Ni1–N1[a]	101.5(1)	N2–Ni1–N7	88.9(1)
N2–Ni1–N7[a]	91.1(1)	N1–Ni1–N7	90.2(1)
N6–H6a···N4	122(7)	N6–H6b···N9[b]	153(6)

Symmetry codes: [a] $-x, -y, -z$. [b] $x, y, z - 1$.

positions are occupied by symmetry-related monodentate N_3^- anions [Ni–N7 2.126(2) and 2.126(3) Å for **3α** and **3β**, respectively]. The dihedral angles between the coordinated pyridyl groups and the triazolato rings are 5.2(4) and 6.7(5)° for **3α** and **3β**, respectively, while those between the noncoordinating pyridyl groups and the triazolate rings are 7.1(4) and 10.2(5) ° for **3α** and **3β**, respectively. There exists intramolecular moderate N–H···N hydrogen bonding interactions between the amine groups and the noncoordinating pyridyl groups [for **3α**: N6···N4 = 2.848(2) Å; N6–H6a···N4 = 141(2)°; for **3β**: N6···N4 = 2.863(5) Å; N6–H4a···N4 = 122(7)°]. What interested us was that the orientations of the linear azide motifs in **3α** and **3β** are quite different, as shown in Figures 3a and 4a. In **3α**, the linear azide motifs run approximately parallel to the long sides of the abpt ligands, while in **3β** the linear azide motifs are approximately perpendicular to the long side of the abpt ligands. Although adjacent monoclinic $[Ni(abpt)_2(N_3)_2]$ motifs are extended via the N–H···N_{azide} [N6···N9^i = 2.966(3) Å, N6–H6b···N9^i = 170(2)° for **3α**; N6···N9^j = 3.095(7) Å, N6–H6b···N9^j = 153(6)° for **3β**; symmetry codes: $i = x, y - 1, z$; $j = x, y, z - 1$] into 1D supramolecular double-stranded chains (Figures 3b and 4b), the dimensions of the cavities in 1D hydrogen-bonded chains of **3α** and **3β** are different. Particularly, the 1D chains are further extended by the nonclassical C–H···N hydrogen bonding (for **3α**: C···N = 3.442 Å and C–H···N = 150.3°; for **3β**: C···N = 3.508 Å and C–H···N = 142.5°) and offset π–π interactions (3.426–3.467 Å) into different 2D molecular layers in **3α** and **3β** (Figure 3c and 4c), and finally resulting in different 3D molecular packings in two polymorphous species. It should be noted that **3α** and **3β** represent a new interesting example showing temperature-induced polymorphism, which was observed in the case of molecular crystals of organic compounds, hydrogen bonded frameworks, and metal complexes such as L-glutamic acid, terpyridine, and $[Cu(Ph_2SNH)_4][PF_6]_2$.[12]

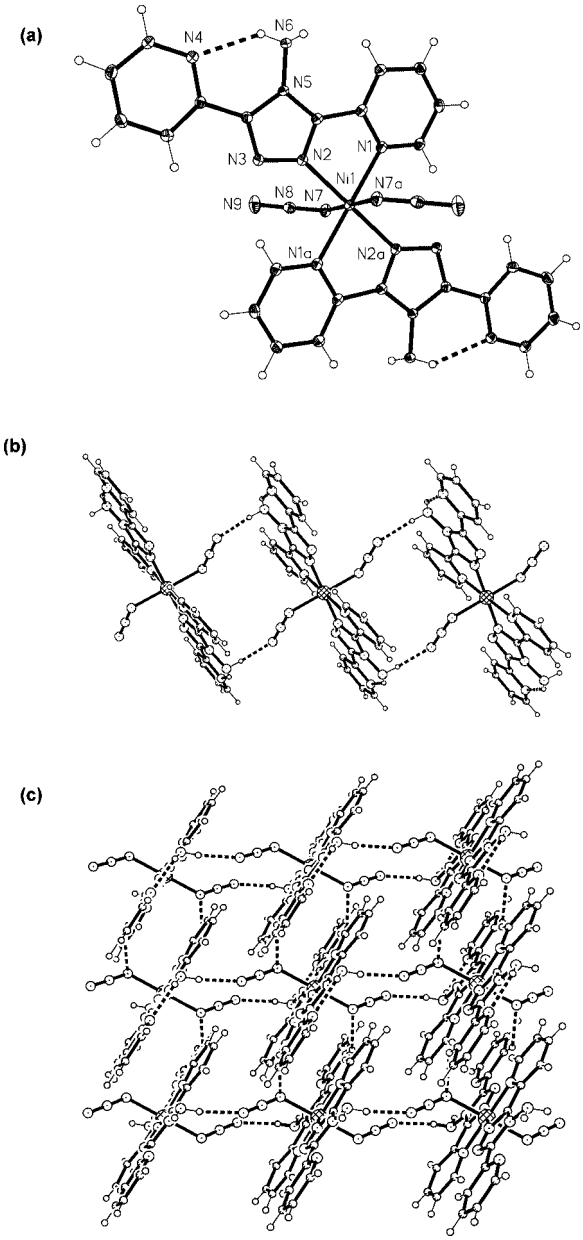

Figure 3. ORTEP plot of the coordination geometry of **3α** (a), the 1D hydrogen-bonded chain (b), and the extension of the 1D chains into 2D molecular layer by interchain π–π and C–H···N interactions in **3α**. 50% thermal ellipsoids are shown.

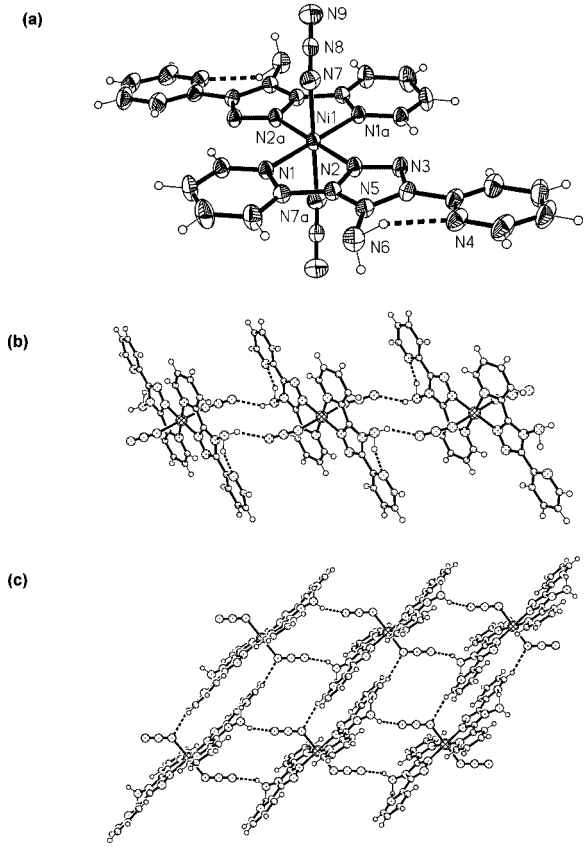

Figure 4. ORTEP plot of the coordination geometry of **3β** (a), the 1D hydrogen-bonded chain (b), and the extension of the 1D chains into 2D molecular layer by interchain π–π and C–H···N interactions in **3β**. 50% thermal ellipsoids are shown.

Magnetic Properties

Magnetic susceptibility data were measured with polycrystalline samples of **1** and **2** in 1.0 KG field over the temperature range of 2–300 K.

For **1**, from room temperature down to 35 K, the $\chi_m T$ product increases continuously and reaches a maximum with 6.56 emu K mol^{-1} (Figure 5). This behavior is indicative of an overall ferromagnetic coupling between the Ni^{II} centers and the low temperature decrease is due to a strong zero-field splitting (ZFS) and/or the presence of a single antiferromagnetic interaction between two of the four Ni^{II} centers. The magnetic data were analyzed with the spin Hamiltonian in Equation (1).

$$\hat{H} = -2J_1\hat{S}_1\hat{S}_2 - 2J_2\hat{S}_2\hat{S}_3 - 2J_3\hat{S}_3\hat{S}_4 - 2J_4\hat{S}_1\hat{S}_4 + D\left(\hat{S}_{z1}^2 + \hat{S}_{z2}^2 + \hat{S}_{z3}^2 + \hat{S}_{z4}^2\right) \quad (1)$$

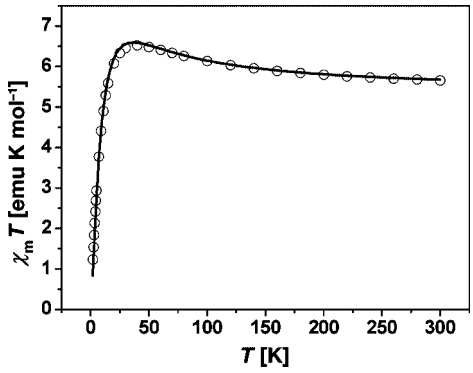

Figure 5. Plot of $\chi_M T$ vs. T for **1**. Solid lines represent the best fit with the parameters given in the text.

Calculations were performed with the magnetism package MAGPACK.[13] The first best fit that was obtained from a least-squares analysis of the $\chi_m T$ implies a very big D value (D = 23.8 cm^{-1}) and unrealistic exchange parameters are J_1 = 2.37 cm^{-1}, J_2 = 4.84 cm^{-1}, J_3 = 15.7 cm^{-1}, J_4 = –3.95 cm^{-1}, and g = 2.31 ($R = 7.5 \times 10^{-4}$). This solution was discarded. In order to reduce the number of parameters, we assumed that the two exchange parameters associated to the azide bridge were equal ($J_1 = J_3$) and the other two exchange parameters associated to the abpt bridge were also equal ($J_3 = J_4$). The best fit implies a zero ZFS and the parameters are $J_1 = J_3$ = 15.3 cm^{-1}, $J_2 = J_4$ = –2.2 cm^{-1}, and g = 2.32. According to this calculation it is found that the ground state is S = 0. Compared with those reported in our recently reported hexanuclear Ni$_6$ circle and other related species,[6] the ferromagnetic interactions (J_1 and J_3) can be assigned to the exchange pathway through the ($\mu_{1,1}$-N$_3$)$_2$(μ-OAc) and ($\mu_{1,1}$-N$_3$)($\mu_{1,1}$-N$_{abpt-H}$)(μ-OAc) bridges. The other two antiferromagnetic interactions can be assigned to the remaining exchange pathways indifferently, which is consistent with the results of X-ray structural analysis. In the future, more compounds of closely related, but significantly different, structures will be needed together with detailed magnetic studies and independent information (ab initio calculations) for a better understanding of magnetic superexchange in this type of compound.

For **2**, the magnetic data (Figure 6) were analyzed with the following spin Hamiltonian: $H = -2JS_1S_2$ ($S_1 = S_2$ = 1). From this Hamiltonian, the equation of magnetic susceptibility can be derived as $\chi = (Ng^2\beta^2/kT)[(5 + e^{4x})/(5 + 3e^{4x} + e^{6x})]$,[3a] in which N, β, and k are fundamental constants, g and J are adjustable parameter, and $x = -J/kT$. The obtained parameters were fitted to be J = –17.62 cm^{-1} and g = 2.19 ($R = 5.1 \times 10^{-4}$). The sign of J in **2** is consistent with the antiferromagnetic J_2 and J_4 coupling via the abpt bridge in **1**.

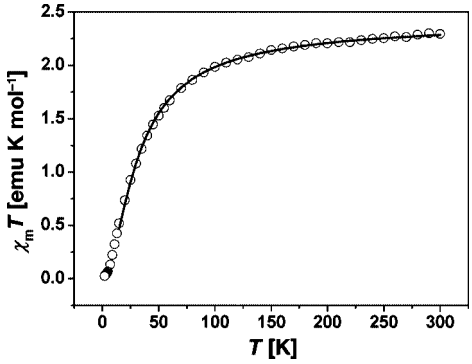

Figure 6. Plot of $\chi_M T$ vs. T for **2**. Solid lines represent the best fit with the parameters given in the text.

Conclusions

In this study, we present new reactivity of 4-amino-3,5-bis(pyridin-2-yl)-1,2,4-triazole to generate a novel tetranuclear nickel(II) rectangle box, a neutral dinuclear species, and a mononuclear species with two polymorphous phases. The μ:η^1:η^2:η^1 coordination mode of the deprotonated [abpt-H]$^-$ ligand in the tetranuclear nickel(II) rectangle box is for the first time observed; the anionic ligand (bpt-H) in the dinuclear nickel(II) complex was generated in situ and resulted from Ni^{II}-assisted deamination. The mononuclear complex represents a new interesting example showing temperature-induced polymorphism. Temperature-dependent magnetic studies revealed the presence of moderate antiferromagnetic coupling via the double μ-abpt bridges in dinuclear complex and the presence of both weak antiferromagnetic coupling via the single μ-abpt bridges and ferromagnetic coupling through the ($\mu_{1,1}$-N$_3$)$_2$(μ-OAc) and ($\mu_{1,1}$-N$_3$)($\mu_{1,1}$-N$_{abpt-H}$)(μ-OAc) bridges, all of which gives an overall ferromagnetic coupling in the tetranuclear complex.

Experimental Section

General Remarks: All reagents were obtained from commercial sources and used as received, unless stated otherwise. 4-Amino-3,5-bis(pyridin-2-yl)-1,2,4-triazole (abpt) was synthesized according to the literature procedure.[14] All preparations and manipulations were performed under aerobic conditions. The C and H microanalyses were carried out with a Various EL elemental analyzer.

Table 5. Crystal data and structure refinement for **1**, **2**, **3α**, and **3β**.

Compound	**1**	**2**	**3α**	**3β**
Formula	$C_{40}H_{45}N_{33}Ni_4O_9$	$C_{26}H_{24}N_{12}Ni_2O_4S_2$	$C_{24}H_{20}N_{18}Ni$	$C_{24}H_{20}N_{18}Ni$
Fw	1366.93	750.11	619.29	619.29
Temperature [K]	123(2)	293(2)	123(2)	293(2)
Crystal system	monoclinic	triclinic	triclinic	triclinic
Space group	*P*2/*c*	$P\bar{1}$	$P\bar{1}$	$P\bar{1}$
a [Å]	21.485(4)	8.389(3)	6.7214(8)	8.497(2)
b [Å]	12.072(2)	8.905(3)	8.321(1)	8.610(2)
c [Å]	21.036(4)	11.710(4)	11.552(1)	10.486(2)
α [°]	90	88.155(5)	95.961(2)	108.930(4)
β [°]	99.399(4)	72.679(5)	95.340(2)	99.064(4)
γ [°]	90	66.709(4)	98.061(2)	104.803(4)
V [Å^3]	5382.8(17)	763.4(4)	632.44(13)	676.9(3)
Z	4	1	1	2
$D_{calcd.}$ [g cm^{-3}]	1.687	1.632	1.626	1.519
μ(Mo-K_α) [mm^{-1}]	1.464	1.426	0.824	0.770
F(000)	2800	384	318	318
No. unique data	26200	6202	3439	5267
No. data with $I > 2\sigma(I)$	10435 (R_{int} = 0.0673)	3276 (R_{int} = 0.0260)	2322 (R_{int} = 0.0114)	2580 (R_{int} = 0.0221)
R_1, wR_2[a] [$I > 2\sigma(I)$]	0.0482, 0.0913	0.0374, 0.0903	0.0303, 0.0747	0.0510, 0.1405
R_1, wR_2[a] (all data)	0.0788, 0.0989	0.0546, 0.0989	0.0326, 0.0762	0.0664, 0.1529

[a] $R_1 = \Sigma||F_o| - |F_c||/\Sigma|F_o|$, $wR_2 = [\Sigma w(F_o^2 - F_c^2)^2/\Sigma w(F_o^2)^2]^{1/2}$, $w = [\sigma^2(F_o)^2 + (0.1(\max(0,F_o^2) + 2F_c^2)/3)^2]^{-1}$.

The FTIR spectra were recorded from KBr pellets in the range 4000–400 cm^{-1} with a Bruker-EQUINOX 55 FTIR spectrometer. Variable-temperature magnetic susceptibility data were obtained from a Quantum Design SQUID MPMS XL-7 magnetometer. The diamagnetism of the sample and sample holder were taken into account and its contributions to the susceptibility were corrected using Pascal's constants. The effective molar magnetic moments were calculated with the equation $\mu_{eff} = 2.828(\chi_M T)^{1/2}$.

$[Ni_4(abpt)_2(abpt\text{-}H)(N_3)_5(O_2CMe)_2]\cdot 5H_2O$ (1): To a methanolic solution (20 mL) of $Ni(O_2CMe)_2\cdot 4H_2O$ (0.120 g, 0.5 mmol) was added a solution of abpt (0.119 g, 0.5 mmol) in the same solvent (20 mL) with magnetic stirring. Once the materials were dissolved, NaN_3 (0.036 mg, 0.5 mmol) was slowly added. The resultant mixture was heated at reflux for 5 h and then filtered. The resulting green solution was then maintained undisturbed at ambient temperature. After 7 d, deep green crystals were collected (yield ca. 52% based on abpt). IR (KBr): $\tilde{\nu}$ = 3449 (s), (br), 3070 (m), 2070 (s), 2041 (vs), 1562 (s), 1493 (s), 1463 (s), 1430 (s), 1342 (w), 1301 (w), 1284 (w), 1258 (m), 1159 (w), 1102 (w), 1056 (w), 1015 (m), 799 (s), 751 (m), 695 (m), 641 (m), 607 (w), 467 (w) cm^{-1}. $C_{40}H_{45}N_{33}Ni_4O_9$ (1366.85): calcd. C 35.25, H 3.32, N 33.82; found C 35.02, H 3.25, N 33.69.

$[Ni_2(bpt\text{-}H)_2(SCN)_2(H_2O)_2]\cdot 2H_2O$ (2): A mixture of abpt (0.056 g, 0.25 mmol) and KNCS (0.186 g, 1.0 mmol) were added to a water/ethanol solution (1:1, 15.0 mL) of $NiCl_2\cdot 6H_2O$ (0.082 g, 0.33 mmol) and stirred. The resultant mixture was heated in a stainless steel reactor with a Teflon liner at 150 °C for 72 h. After a period of approximately 14 h cooling to room temp., green block-like crystals were obtained, isolated simultaneously by filtration, and washed with water (yield: 29%). IR (KBr): $\tilde{\nu}$ = 3745 (m), 3343 (w), 3071 (m), 2934 (m), 2358 (m), 2108 (m), 2058 (s), 1608 (s), 147 (m), 1415 (m), 1267 (m), 1152 (s), 1050 (m), 777 (s), 731 (m), 633 (s) cm^{-1}. $C_{26}H_{24}N_{12}Ni_2O_4S_2$: calcd. C 41.64, H 3.23, N 22.41; found C 41.25, H 3.10, N 22.32.

α-$[Ni(abpt)_2(N_3)_2]$ (3α): The synthetic method was similar to that of **1** by using 1:2:2 molar ratio of Ni^{2+}/abpt/N_3^- (yield 65%). IR (KBr): $\tilde{\nu}$ = 3331 (m), 3204 (s), 3116 (m), 2034 (s), 1639 (s), 1605 (s), 1590 (s), 1569 (s), 1491 (s), 1456 (s), 1426 (s), 1302 (s), 1254 (s), 1167 (s), 1047 (m), 1015 (s), 976 (s), 785 (s), 745 (s), 697 (s) cm^{-1}. $C_{24}H_{20}N_{18}Ni$: calcd. C 46.55, H 3.26, N 40.71; found C 46.42, H 3.20, N 40.53.

β-$[Ni(abpt)_2(N_3)_2]$ (3β): A mixture of abpt (0.120 g, 0.5 mmol) and NaN_3 (0.036 g, 0.5 mmol) were added to an aqueous solution (15.0 mL) of $Ni(O_2CMe)_2\cdot 4H_2O$ (0.060 g, 0.25 mmol) and stirred. The resultant mixture was heated in a stainless steel reactor with a Teflon liner at 130 °C for 72 h. After a period of approximately 14 h cooling to room temp., green block-like crystals were obtained (yield: 21%). IR (KBr): $\tilde{\nu}$ = 3337 (m), 3223 (s), 3128 (m), 2053 (s), 1638 (s), 1613 (s), 1578 (s), 1557 (s), 1487 (s), 1498 (s), 1426 (s), 1302 (s), 1258 (s), 1188 (s), 1060 (m), 1025 (s), 998 (s), 774 (s), 765 (s), 666 (s), 601 (s), 426 (s) cm^{-1}. $C_{24}H_{20}N_{18}Ni$: calcd. C 46.55, H 3.26, N 40.71; found C 46.47, H 3.22, N 40.36.

Safety Note: *Azide salts of metal complexes with organic ligands are potentially explosive. Only small amounts of material should be prepared and these should be handled with great caution.*

X-ray Crystallographic Study: Diffraction intensities of **1**, **2**, **3α**, and **3β** were collected with a Bruker Apex CCD area-detector diffractometer (Mo-K_α, λ = 0.71073 Å). For data reduction the "Bruker Saint Plus" program was used.[15] Data were corrected for Lorentz and polarization effects; empirical absorption correction was applied by using multiscan program SADABS.[16] The structures were solved with direct methods and refined with a full-matrix least-squares technique with the SHELXTL programs.[17] Non-hydrogen atoms were refined anisotropically. The positions of the hydrogen atoms for the carbon atoms were calculated assuming ideal geometries, while those for the amino, imino groups, and water molecules are located from the difference Fourier map and refined with isotropic temperature factors. A summary of the data collection and structure refinement information is provided in Table 5. Drawings were produced with SHELXTL.[18]

CCDC-285539 (for **1**), -285540 (for **2**), -294286 (for **3α**), and -294287 (for **3β**) contain the supplementary crystallographic data for this paper. These data can be obtained free of charge from The Cambridge Crystallographic Data Centre via www.ccdc.cam.ac.uk/data_request/cif.

Acknowledgments

This work was supported by the NSFC (No. 20525102 and 20471069), the FANEDD of China (200122), SRFDP (20060558081), and the Scientific and Technological Project of Guangdong Province (04205405). The authors are grateful to Prof. Jin-Lin Zuo for fruitful discussions.

[1] J. S. Miller and M. Drillon (Eds.), *Magnetism: Molecules to Materials II: Molecule-Based Materials*, Wiley-VCH, Weinheim, Germany, **2001**.

[2] a) J. Ribas, A. Escuer, M. Monfort, R. Vicente, R. Cortés, L. Lezama, T. Rojo, *Coord. Chem. Rev.* **1999**, *193–195*, 1027–1068; b) A. K. Boudalis, B. Donnadieu, V. Nastopoulos, J. M. Clemente-Juan, A. Mari, Y. Sanakis, J.-P. Tuchagues, S. P. Perlepes, *Angew. Chem. Int. Ed.* **2004**, *43*, 2266–2270; c) A. Escuer, G. Aromí, *Eur. J. Inorg. Chem.* **2006**, 4721–4736.

[3] a) F. S. Keij, R. A. G. de Graaff, J. G. Haasnoot, J. Reedijk, *J. Chem. Soc. Dalton Trans.* **1984**, 2093; b) J.-C. Chen, S. Hu, A.-J. Zhou, M.-L. Tong, Y.-X. Tong, *Z. Anorg. Allg. Chem.* **2006**, *632*, 475–481; c) J.-C. Chen, A.-J. Zhou, S. Hu, M.-L. Tong, Y.-X. Tong, *J. Mol. Struct.* **2006**, *794*, 225–229; d) M.-X. Peng, C.-G. Hong, C.-K. Tan, J.-C. Chen, M.-L. Tong, *J. Chem. Crystallogr.* **2006**, *36*, 703–707.

[4] a) P. J. Kunkeler, P. J. van Koningsbruggen, J. P. Cornelissen, A. N. van der Horst, A. M. van der Kraan, A. L. Spek, J. G. Haasnoot, J. Reedijk, *J. Am. Chem. Soc.* **1996**, *118*, 2190–2197; b) N. Moliner, A. B. Gaspar, M. C. Munoz, V. Niel, J. Cano, J. A. Real, *Inorg. Chem.* **2001**, *40*, 3986–3991; c) N. Moliner, M. C. Munoz, S. Létard, J.-F. Létard, X. Solans, R. Burriel, M. Castro, O. Kahn, J. A. Real, *Inorg. Chim. Acta* **1999**, *291*, 279–288; d) A. B. Gaspar, M. C. Muñoz, N. Moliner, V. Ksenofontov, G. Levchenko, P. Gütlich, J. A. Real, *Monatsh. Chem.* **2003**, *134*, 285.

[5] a) J. G. Haasnoot, *Coord. Chem. Rev.* **2000**, *200–202*, 131–185; b) M. H. Klingele, S. Brooker, *Coord. Chem. Rev.* **2003**, *241*, 119–132; c) P. J. van Koningsbruggen, D. Gatteschi, R. A. G. de Graaff, J. G. Haasnoot, J. Reedijk, C. Zanchini, *Inorg. Chem.* **1995**, *34*, 5175–5182.

[6] M.-L. Tong, M. Monfort, J. M. Clemente Juan, X.-M. Chen, X.-H. Bu, M. Ohba, S. Kitagawa, *Chem. Commun.* **2005**, 233–235, and references cited therein.

[7] F. Meyer, P. Kircher, H. Pritzkow, *Chem. Commun.* **2003**, 774–775.

[8] a) M. P. Garcia, J. A. Manero, L. A. Oro, M. C. Apreda, F. H. Cano, C. Foces-Foces, J. G. Haasnoot, R. Prins, J. Reedijk, *Inorg. Chim. Acta* **1986**, *122*, 235–241; b) H. M. Burke, J. F. Gallagher, M. T. Indelli, J. G. Vos, *Inorg. Chim. Acta* **2004**, *357*, 2989–3000.

[9] a) J.-P. Zhang, Y.-Y. Lin, X.-C. Huang, X.-M. Chen, *J. Am. Chem. Soc.* **2005**, *127*, 5495–5506; b) J.-P. Zhang, Y.-Y. Lin, X.-C. Huang, X.-M. Chen, *Chem. Commun.* **2005**, 1258–1260.

[10] X.-M. Chen, M.-L. Tong, *Acc. Chem. Res.* **2007**, *40*, 162–170.

[11] a) S. Supriya, S. K. Das, *New J. Chem.* **2003**, *27*, 1568–1574; b) J. Tao, Z.-J. Ma, R.-B. Huang, L.-S. Zheng, *Inorg. Chem.* **2004**, *43*, 6133–6135; c) S. Pal, N. B. Sankaran, A. Samanta, *Angew. Chem. Int. Ed.* **2003**, *42*, 1741–1743.

[12] a) G. S. McGrady, M. Odlyha, P. D. Prince, J. W. Steed, *CrystEngComm* **2002**, *4*, 271–276; b) S. A. Barnett, A. J. Blake, N. R. Champness, *CrystEngComm* **2003**, *5*, 134–136; c) K. E. Holmes, P. F. Kelly, M. R. J. Elsegood, *CrystEngComm* **2004**, *6*, 56–59; d) K. E. Holmes, P. F. Kelly, S. H. Dale, M. R. J. Elsegood, *CrystEngComm* **2006**, *8*, 391–402; e) J. M. Kelleher, S. E. Lawrence, M. T. McAuliffe, H. A. Moynihan, *CrystEngComm* **2007**, *9*, 72–77.

[13] a) J. J. Borrás-Almenar, J. M. Clemente-Juan, E. Coronado, B. S. Tsukerblat, *Inorg. Chem.* **1999**, *38*, 6081–6088; b) J. J. Borrás-Almenar, J. M. Clemente-Juan, E. Coronado, B. S. Tsukerblat, *J. Comput. Chem.* **2001**, *22*, 985–989.

[14] J. F. Geldard, F. Lions, *J. Org. Chem.* **1965**, *30*, 318–321.

[15] *SMART Version 5.625 and SAINT+ Version 6.02a*, Bruker Analytical X-ray Systems, Inc., Madison, Wisconsin, US, **1998**.

[16] G. M. Sheldrick, *SADABS 2.05*, University Göttingen.

[17] *SHELXTL 6.10*, Bruker Analytical Instrumentation, Madison, Wisconsin, USA, 2000.

[18] G. M. Sheldrick, *SHELXTL Version 5*, Siemens Industrial Automation Inc., Madison, Wisconsin, US, **1995**.

Received: March 16, 2007
Published Online: June 21, 2007

